Soil Subsurface Channel Statistical Characterization for Drone-Borne Intelligent GPR Advancement

Noushin Khosravi Largani
Data Science Department
Worcester Polytechnic Institute (WPI)
Worcester, MA, USA
nlargani@wpi.edu

Seyed (Reza) Zekavat
Data Science Department
Worcester Polytechnic Institute (WPI)
Worcester, MA, USA
rezaz@wpi.edu

Vincent Filardi
Data Science Department
Worcester Polytechnic Institute (WPI)
Worcester, MA, USA
vfilardi@wpi.edu

***Abstract*—The advancement of drone-borne intelligent Ground Penetration Radar (GPR) is hinged upon accurate received signal feature extraction, which relies on high-performance soil subsurface channel estimation. This requires the optimal design of the transmitted waveform, which needs soil subsurface channel parameter statistics. In this paper, we investigate the statistics of soil subsurface channel parameters for different soil textural classes (defined by sand and clay percentage, and adopted based on the USDA textural triangle). Channel parameters statistics of interest are the gain correlation matrices, the statistical distributions of gain and Time-of-Arrival (ToA), and the mean Power-Delay Profile (PDP). Channel gain correlation matrix and its distribution are critical to waveform design. Mean PDP offers insight into the number of soil layers. The results of this paper contribute to the intelligent optimal waveform design for GPR, the implementation of feature extraction in ML applications, and accurate estimation of soil layers, moisture, and permittivity.**

***Index Terms*—GPR Channel Statistics, Waveform Design, Soil Subsurface, Emulation Parameter Selection**

I. Introduction

Drone-borne Ground penetration radar (GPR) is one of the most effective and ubiquitous tools for noninvasive soil subsurface characterization of large-scale land areas, making it applicable to numerous fields including civil engineering, environmental studies, archaeology, and agriculture [1], [2]. To extract the subsurface features such as permittivity, conductivity, and the number of layers efficiently, GPR transmits a signal over a wide frequency spectrum through the ground and records the received reflections. The received GPR signal is formed by an interaction between the transmitted waveform and the soil subsurface channel. A key parameter to characterize soil subsurface channel is its impulse response that includes an array of Time-of-Arrivals (ToAs) and their associated coefficients, known as channel gains [3], [4].

Optimal waveform design involves high-performance impulse response parameter estimation that in turn enhances the estimation of soil subsurface features such as texture, and moisture content. Optimal waveform design requires prior knowledge of the channel parameters' statistics such as the mean, covariance, correlation matrix, and distribution of channel gains [5]–[9]. Moreover, soil subsurface investigation in modern agricultural analysis is increasingly conducted using advanced machine learning (ML) techniques [10]–[12]. To optimize ML feature extraction from the received GPR signal and improve the performance of ML models, a thorough understanding of the soil channel parameters' statistical properties is of utmost importance.

Soil channel characterization has been explored from different aspects in the existing literature, offering an understanding of its applications and complexities. The authors of [13], [14] study soil channels where both transmitter and receiver are located in the soil medium. In [15], the soil-air channel is assessed to achieve a precision irrigation system. However, [13]–[15] do not offer detailed knowledge about channel statistics. In [16] and [17], air-soil channel statistics such as coherence bandwidth and the distribution of received signal magnitude are examined, respectively. The impact of soil parameters on the soil channel statistics in underground channels has been comprehensively investigated [4].

Although the mentioned studies thoroughly characterize the soil channel, they are not sufficient to entirely encompass soil channel investigation in air-coupled GPR scenarios. Because all of them follow an invasive approach, in which either or both of the transmitting and receiving antennas are buried in the soil. Accordingly, the distribution obtained for channel gains and other channel parameters cannot be applied to GPR systems. In addition, none of them have obtained and analyzed the correlation coefficients of soil channel gains, which is the most essential prerequisite for waveform design.

This paper studies air-coupled GPR statistical assessment of soil channel that is critical to GPR optimal waveform design. Here, we evaluate soil channel parameters' statistics for each of the three soil classes (i.e., silt loam, sand, and clay), represented at the corners of the USDA textural triangle. For each soil class, We have obtained more than 700 GPR signals. For each GPR received signal, we acquire the soil subsurface channel impulse response parameters (channel gains and ToAs). Then, we extract the statistics of the mentioned parameters that include the channel gain correlation matrices, the statistical distributions of channel gain and ToA, as well as mean Power-Delay Profile (PDP). Among these statistics, the correlation matrix and distribution of channel gains have the most impact on optimal waveform creation. The paper highlights the impact

This research is funded by the United States Department of Agriculture (Grant Number: USDA NR223A750013G032). We are deeply thankful for their financial support of this work.

of soil subsurface texture on the statistics, and provides insight into how optimum waveform design should be implemented for soil subsurface channel assessment. The results of this paper contribute to the intelligent optimal waveform design for GPR, support the implementation of feature extraction in ML applications, and, provide insights on how to utilize the observed high cross-correlation among the channel gains for feature selection in ML models.

Soil subsurface channel is introduced in Sections II. Channel statistical feature characterization, emulation parameter selection, results and discussions, and conclusions are presented in Sections III, IV, V and VI, respectively.

II. Soil Subsurface Channel

The GPR-transmitted signal travels through the soil medium and interacts with the properties of the soil. The soil channel statistical characteristics, measured via the GPR received signal, vary with the waveform's features such as carrier frequency and spectrum, and the soil's physical characteristics, including texture, bulk density, particle density, moisture, number of layers, and the depth per layer, which are described in the following. High-resolution soil subsurface channel impulse response evaluation requires a waveform with a large frequency bandwidth. Hence, the transmitted waveform shall consist of multiple frequency components. Each frequency component is attenuated differently with the soil channel. For example, high-frequency components may constitute higher attenuation compared to low-frequency components. In addition, soil medium alters the speed of propagation differently at each frequency component. Thus, a wider waveform spectrum (bandwidth) includes more information content about the soil channel. This makes wider spectrum waveforms more suitable for ML applications.

According to the USDA textural triangle (Fig. 1), the soil texture (i.e., percentage of sand, clay, and silt) is categorized into twelve types such as silt loam, sand, clay, etc. Soil's bulk density refers to the mass of dry soil per unit volume of soil and air. Soil's particle density represents the mass of dry soil per unit volume of soil particles only (without air) [19]. The soil's texture, bulk density, and particle density influence the signal's attenuation and channel statistics. In general, as the sand percentage increases and that of clay decreases, signal attenuation decreases. The reason is that sand has the lowest and clay has the highest capacity for water holding, which is due to the sand's large and clay's small pore space. Water holding is an element showing the electromagnetic wave absorption by soil [4], [19]. Smaller pore space indicates higher bulk density [19], [20]. Silt loam falls between sand and clay in terms of the properties mentioned [4]. Particle density is almost the same for different textural classes of soil. Higher particle density indicates greater compactness of soil particles, which leads to increased signal attenuation [20].

As the signal travels deeper into the soil layer, it gets more attenuated. In addition, the heterogeneous nature of soil leads to receiving multiple reflections of the transmitted signal at the receiver, where the reflections may strengthen or weaken each other [4]. Increasing the number of layers is the other reason for receiving multiple reflections [3]. Due to the signal absorption by water molecules, the signal strength is reduced as it propagates through moist soils [19]. Moisture is regarded as the dominant factor that determines soil permittivity. Specifically, [21] has offered the empirical relationship for effective permittivity κ of a material composing of different components such as soil, water, air, represented by:

$$\kappa = \left[(1-\eta)\sqrt{k_s} + (\eta - VWC)\sqrt{k_a} + VWC\sqrt{k_w}\right]^2, \tag{1}$$

in which dielectric permittivity of soil, air, and water are denoted by k_s, k_a, and k_w, respectively. The parameters η and VWC represent the soil porosity and the free soil water content, respectively. As k_w is approximately 81 within the GPR frequency range, while $k_a = 1$ and k_s ranges from 4 to 7, the dominant impact of water volume percentage on the effective permittivity can be inferred [22].

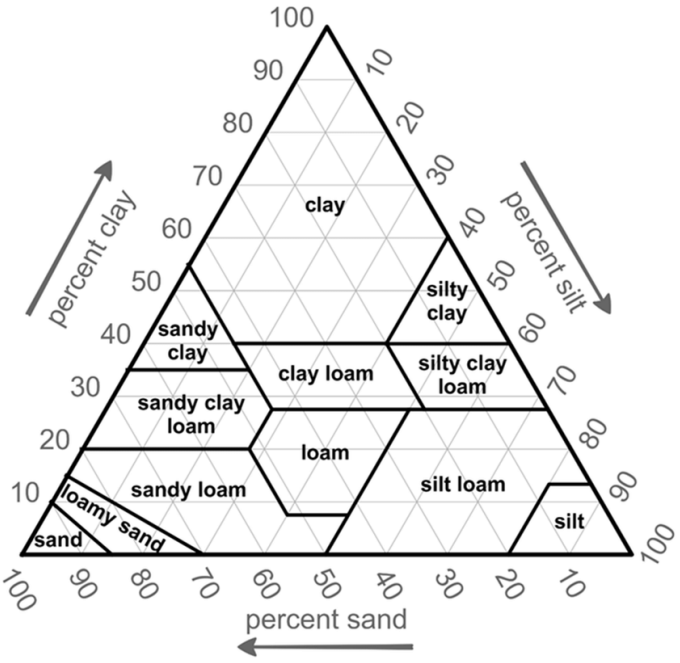

Fig. 1. USDA textural triangle [18]

III. Soil Channel Statistical Characterization

This section presents the applied post-processing method for extracting soil channel impulse response (SCIR) using time-domain GPR received signals. The soil medium serves as a channel between the GPR transmitter and receiver, characterized by a time-domain SCIR that corresponds to:

$$h(t) = \sum_{l=1}^{L} a_l \delta(t - \tau_l), \tag{2}$$

where a_l and τ_l represent complex channel gains and ToAs, respectively. Here, L represents the number of multiple reflec-

tions [3], [4]. The relationship between the transmitted and received signals in the frequency domain is:

$$Y = HX + N, \tag{3}$$

in which H, N, X, and Y indicate the Fourier transform of SCIR, noise, transmitted signal, and received signal, respectively. The extracted SCIR is depicted in the frequency domain as $H = \frac{Y}{X}$ [3]. Applying the Inverse Fourier Transform, the SCIR in time domain $h(t)$ is acquired.

Here, we evaluate mean, correlation matrix, and distribution of channel gains, distribution of ToAs, and mean PDP statistics of soil channel. The mean of channel gains are correspond to:

$$E\{a_l\} = \frac{1}{N}\sum_{n=1}^{N} a_{l,n}, \tag{4}$$

where N refers to the number of GPR received signals for each soil type. $a_{l,n}$ is the nth extracted a_l, where $n = 1 : N$ and $l = 1 : L$. As mentioned, L is the number of multiple reflections. The elements of the covariance matrix of channel gains are expressed as:

$$\text{CoV}\{a_l, a_{l'}\} = \frac{1}{N-1}\sum_{n=1}^{N} \left(a_{l,n} - E\{a_l\}\right)\left(a_{l',n} - E\{a_{l'}\}\right), \tag{5}$$

in which $a_{l',n}$ denotes nth extracted $a_{l'}$ for $l' = 1 : L$. The elements of the correlation matrix are represented by:

$$\rho_{a_l, a_{l'}} = \frac{\text{CoV}\{a_l, a_{l'}\}}{\sigma_{a_l}\sigma_{a_{l'}}}, \tag{6}$$

in which σ_{a_l} and $\sigma_{a_{l'}}$ indicate standard deviation of a_l and $a_{l'}$, respectively. Mean PDP illustrates the average received power for each delay bin, which is determined by the transmitted signal's bandwidth [4]. The distribution of channel gains and ToAs are extracted in terms of cumulative distribution function (CDF).

IV. Emulation Parameter Selection

We use gprMax to emulate a large number of synthetic GPR received signals for each soil class (i.e., silt loam, sand, and clay), and then extract the SCIR statistics specific to each class. gprMax software is a strong emulation tool that employs the Finite Difference time domain (FDTD) method to create synthetic GPR received signals [23]. This software has been used for GPR synthetic data creation in numerous studies [11], [24]–[26]. gprMax uses the Peplinski model to emulate soil medium, which requires the soil parameters including the percentage of sand, the percentage of clay, bulk density, particle density, and moisture range (minimum and maximum moisture percentage). We create the geometric area (polygon) of each textural class (silt loam, sand, and clay) based on the USDA textural triangle (Fig. 1). Then, within each polygon area, we randomly select the percentages of sand and clay to introduce variability and randomness in the soil texture. By repeatedly selecting different percentages of sand and clay within each polygon area and conducting simulations accordingly, we generate a large number of output files for each soil class, from which we then extract statistics. Since the moisture content plays the dominant role in affecting the soil's permittivity [22], we set it to a low value (such as 5% [22]) to be able to observe the impact of soil's texture on the soil channel statistics. Accordingly, the minimum and maximum moisture percentages are chosen to be 5 and 6, respectively. Given the consistent particle density across different soil classes, approximately 2.66 grams per cubic centimeter as noted in [20], we have set the particle density to this value in our analysis. To highlight the impact of textural class on soil channel statistics, we maintained a consistent bulk density across all soil classes, setting it at 1.33 grams per cubic centimeter. This value is included within the bulk density range typical for all soil classes [27], [28].

The Peplinski model works in a frequency range of 300 MHz to 1300 MHz [29]. For soil illumination, we select the Ricker waveform, which is commonly employed in GPR inspections and closely resembles the GPR pulses [24]. The Ricker waveform's center frequency (f_c) is established at 825 MHz, leading to the minimum (f_{min}) and maximum (f_{max}) frequencies to be 375.168 MHz and 1274.831 MHz, respectively (according to the equations provided in [30]). Hence, the transmitted waveform's frequency is contained in the acceptable frequency range for the Peplinski model. Accordingly, the system's bandwidth and range resolution are 899.663 MHz and 17 cm, respectively. The depth of the soil medium (along the z dimension) is set to be more than the range resolution (20 cm in our emulations).

To select an appropriate size for the surface of the soil medium (x-y plane), we conduct an additional series of emulations where the setup and all parameters remain constant, and only the surface dimensions (x and y) change for each emulation run. The channel gains vector is extracted for each emulation. In different emulations, the surface size is incrementally increased, and we calculate the Euclidean distance between the channel gains vector associated with each x-y size and the immediately larger x-y size. The Euclidean distance is normalized to the size of the channel gains vector associated with the larger surface size and is obtained in terms of percentage, which is our defined error measure. As the surface size increases, the error measure decreases, but the required time and memory also increase. To maintain a trade-off between accuracy and time-memory efficiency, we choose a size providing an acceptable value for the error measure. The emulations reveal that to achieve an error of 10 percent or less while efficiently using time and memory, the appropriate surface size is x = y = 120 cm, approximately around $1.5\lambda_{max}$, where $\lambda_{max} = \frac{C}{f_{min}}$ and C is the speed of light.

To capture multiple reflections from the soil, we choose a dipole antenna for its omnidirectional radiation pattern. The dipole antenna is positioned centrally on the x-y plane, consistent with its radiation pattern [31]. The height of the dipole antenna is set to be 41 cm (more than $\frac{\lambda_{max}}{2}$) from the soil surface, which is within the dipole antenna's intermediate-field region and results in desired outputs [31]. The FDTD pixel size (Δl) in gprMax is determined based on the minimum

wavelength. More specifically, $\Delta l \leq \frac{\lambda_{min}}{10}$, where $\lambda_{min} = \frac{C}{f_{max}\sqrt{\epsilon_{r,\max}}}$ and $\epsilon_{r,\max}$ denotes the maximum permittivity of the medium. Considering that water, with a permittivity of approximately 80, is included in our soil medium simulations and represents the maximum permittivity, we set $\Delta l = 0.0008$ in our emulations.

V. Results and Discussions

We obtain more than 700 GPR received signal samples corresponding to each three classes of soil, i.e., sand, silt loam, and clay as shown in Fig. 1. These samples are used to compute the soil channel statistics. The percentage of sand and clay in each soil class region are selected such that each point within that region is adopted with a uniform probability. All emulations consider the same moisture, bulk density, and particle density.

Fig. 2 depicts the mean PDPs of silt loam, sand, and clay. The peak power of the reflection from the soil surface is 0.004, which is approximately eight times higher than that of reflections from the inside of the soil, at 0.0005. This indicates that multiple reflections from inside the soil are significantly weaker due to attenuation, a factor that must be considered when configuring the receiver's dynamic range. The two clusters in Fig. 2 represent the reflections from the soil surface and reflections from the inside of the one-layer soil. Hence, the number of clusters in the mean PDP indicates the number of layer interfaces, offering insights into the layer structure. Moreover, identifying these clusters enriches the interpretation of the correlation matrix for channel gains, as will be discussed next.

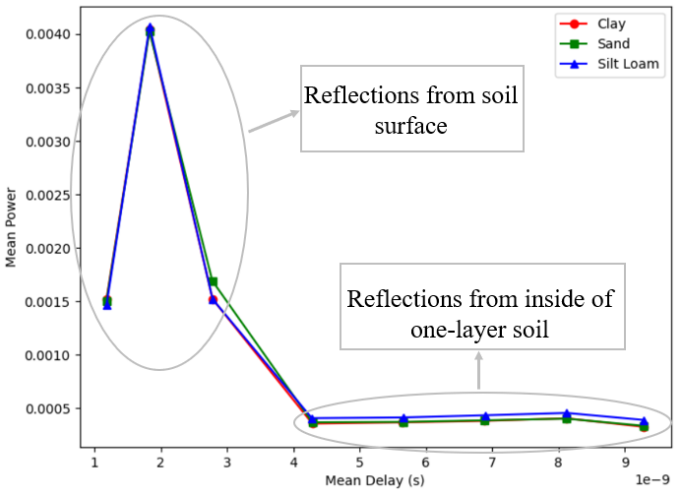

Fig. 2. Mean PDP for silt loam, sand, and clay

Fig. 3 presents the correlation matrix (indicated as correlation heatmap) of the channel gains for sand. The correlation matrix is extracted for silt loam, sand, and clay, with all three displaying similar patterns. The number of resolvable reflections is eight. Hence, the channel gains are a_1 to a_8, with a correlation matrix of 8×8. Here, we define the following measures for correlation based on the absolute value of a cross-correlation coefficient: *highly correlated*, if greater than 0.7, *slightly correlated* if between 0.3 and 0.7, and *uncorrelated* if less than 0.3. Accordingly, the correlation matrix indicates that the channel gains associated with the second cluster in Fig. 2, i.e., the reflections from the inside of the soil are highly correlated. The high cross-correlation (close to one) among the channel gains from reflections within the soil cluster suggests that they share the same information. Knowing one of these values provides nearly all the information content. Therefore, for a downstream ML model (see [32]), it is sufficient to use only one channel gain from this group as a feature. Furthermore, we extract the mean of the absolute values of channel gain cross-correlations for sand, silt loam, and clay, with clay showing the highest value (0.97) and sand the lowest (0.88). The reason is that sand has the largest and most irregular particles, leading to greater randomness, while clay exhibits the opposite characteristics. This observation highlights that the mean of the absolute values of channel gain cross-correlations can be used as a feature for texture detection using GPR-received signals. Moreover, as mentioned in the introduction, channel gain statistics are critical to optimal waveform design. The results depicted in Fig. 3 highlight that the channel gains are highly correlated. Based on the classical theoretical foundations of optimal waveform design (see [5]–[7]), if the channel gains are correlated, optimal waveform design requires the availability of the channel gain distributions.

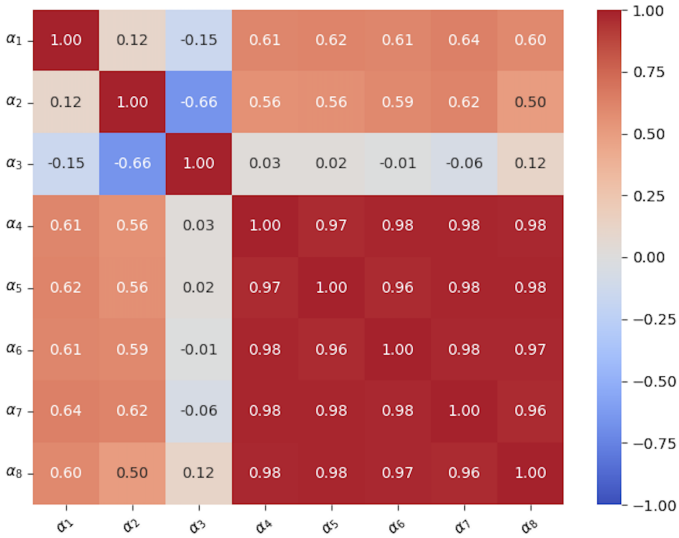

Fig. 3. Correlation heatmap for channel gains of sand

Fig. 4 shows the empirical and fitted Cumulative Distribution Function (CDF) curves of channel gains for silt loam. The curve follows a Normal distribution. In addition, the CDFs for sand and clay follow a Normal distribution. The Normal distribution for the soil channel facilitates a straightforward approach for optimal waveform design [5]–[9]. Given the distribution of each gain is normal, with the assumption of jointly Normal distribution, the overall probabilistic behavior

of the channel gain vector can be determined based on the correlation matrix and mean information, which is key to optimal waveform design. It should be noted that the high cross-correlation between the elements of the Normally distributed channel gain's vector can be leveraged for the implementation of ML models, which can estimate all gains based on the availability of one gain. This is a basis for the simplification of the computation process of optimal waveforms.

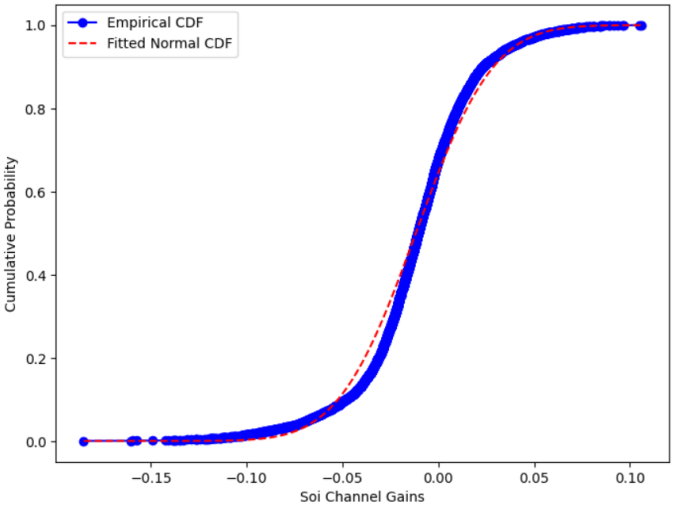

Fig. 4. Empirical and fitted Normal CDF of silt loam

The absolute values for mean and standard deviation (std) of the CDF of soil channel gains for sand, silt loam, and clay are shown in Table I. The table results show that the mean and std values of channel gains' CDF for sand, silt loam, and clay are close to each other. Hence, these values are unlikely to serve as effective features for distinguishing soil texture during ML training.

TABLE I
MEAN AND STANDARD DEVIATION FOR DIFFERENT SOIL TEXTURES

Texture	Mean	Std
Sand	0.009	0.032
Silt loam	0.012	0.032
Clay	0.011	0.031

Fig. 5 indicates the CDF of ToAs for clay. The CDF of ToAs for silt loam and sand are extracted as well. This feature is useful in the selection of optimal bandwidth and pulse duration for the transmitted signal, leading to resolution maximization and interference minimization. The CDF of ToAs for clay is completely similar to that of silt loam and sand. Due to this similarity, the CDF of ToAs is unlikely to serve as a suitable feature for texture classification in ML applications as well.

VI. CONCLUSIONS

The paper extracts the statistics of soil channel for three corners of the USDA textural triangle, i.e., silt loam, sand, and clay under the same condition for moisture. The moisture levels are kept low to minimize its significant impact on wave

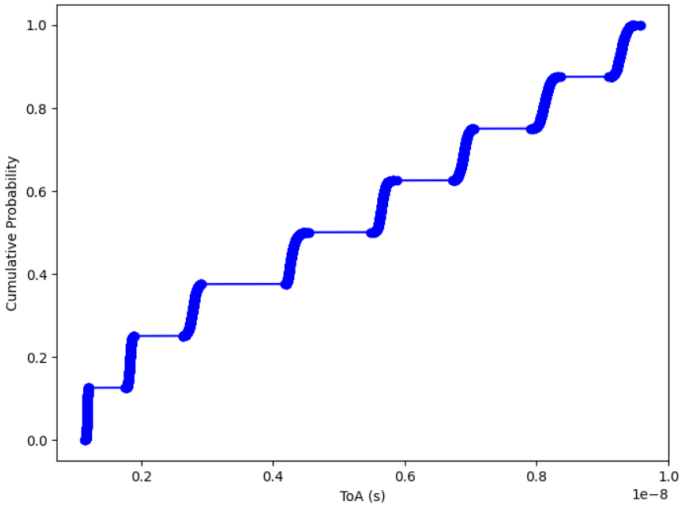

Fig. 5. CDF of ToAs for clay

propagation through the soil. The extracted statistics include the gain correlation matrices, the statistical distributions of gain and ToA, as well as mean PDP. We show that according to the observed high cross-correlation among channel gains from soil reflections, they convey nearly identical information, and using a single channel gain from this group as a feature for ML training is sufficient. In addition, we indicate that the empirical distribution of channel gains follows a Normal distribution, allowing straightforward optimal waveform design and implementation of ML models for soil channel estimation. We show that the mean of the absolute values of channel gain cross-correlations can be used as a feature for texture detection using GPR-received signals. On the other hand, ToA, and the mean and std of channel gains' CDF are unlikely to serve as effective features for distinguishing soil textures in ML applications. The presented results are applicable in areas such as waveform design and consequently accurate estimation of soil layers, moisture, and permittivity. Moreover, our statistical analysis provides useful insights into the feature engineering area of ML applications. This research is critical to our future directions for the development of optimal waveform for various soil texture and moisture conditions.

REFERENCES

[1] P. A. Ryazantsev, A. E. Hartemink, and O. N. Bakhmet, "Delineation and description of soil horizons using ground-penetrating radar for soils under boreal forest in Central Karelia (Russia)," Catena, vol. 214, p. 106285, July 2022.

[2] M. Zajc, J. Urbanc, U. Pečan, M. Glavan, and M. Pintar, "Using 3D GPR for determining soil conditions in precision agriculture," in 18th International Conference on Ground Penetrating Radar, pp. 291–294, Society of Exploration Geophysicists, 2020.

[3] S. Zheng, X. Pan, A. Zhang, Y. Jiang, and W. Wang, "Estimation of echo amplitude and time delay for OFDM-based ground-penetrating radar," IEEE Geoscience and Remote Sensing Letters, vol. 12, no. 12, pp. 2384–2388, 2015.

[4] A. Salam, M. C. Vuran, and S. Irmak, "A statistical impulse response model based on empirical characterization of wireless underground channels," IEEE Trans. Wireless Commun., vol. 19, no. 9, pp. 5966–5981, 2020.

[5] M. B. Mashhadi and D. Gündüz, "Pruning the pilots: Deep learning-based pilot design and channel estimation for MIMO-OFDM systems," IEEE Trans. Wireless Commun., vol. 20, no. 10, pp. 6315–6328, 2021.
[6] V. Karimi, R. Mohseni, and S. Samadi, "Adaptive OFDM waveform design for cognitive radar in signal-dependent clutter," IEEE Syst. J., vol. 14, no. 3, pp. 3630–3640, 2019.
[7] F. Rottenberg, F. Horlin, E. Kofidis, and J. Louveaux, "Generalized optimal pilot allocation for channel estimation in multicarrier systems," in Proc. IEEE 17th Int. Workshop Signal Process. Adv. Wireless Commun. (SPAWC), 2016, pp. 1–5.
[8] M. R. Bell, "Information theory and radar waveform design," IEEE Trans. Inf. Theory, vol. 39, no. 5, pp. 1578–1597, 1993.
[9] Y. Yang and R. S. Blum, "MIMO radar waveform design based on mutual information and minimum mean-square error estimation," IEEE Trans. Aerosp. Electron. Syst., vol. 43, no. 1, pp. 330–343, 2007.
[10] S. K. Pramanik, M. S. Hossain, and S. M. Islam, "Non-contact soil moisture estimation using continuous wave radar and deep learning," IEEE Sensors J., 2024.
[11] H. Namdari, M. Moradikia, R. Askari, O. Mangoubi, D. Petkie, and S. Zekavat, "Advancing precision agriculture: Machine learning-enhanced GPR analysis for root-zone soil moisture assessment in mega farms," IEEE Trans. Agrifood Electron., accepted for publication, 2024.
[12] V. Filardi, A. Cheung, R. Khan, O. Mangoubi, M. Moradikia, S. R. Zekavat, B. Wilson, R. Askari, and D. Petkie, "Data-driven soil water content estimation at multiple depths using SFCW GPR," in Proc. IEEE Int. Opportunity Res. Scholars Symp. (ORSS), 2023, pp. 86–90.
[13] X. Dong and M. C. Vuran, "A channel model for wireless underground sensor networks using lateral waves," in Proc. IEEE Globecom '11, Houston, TX, Dec. 2011.
[14] M. C. Vuran and I. F. Akyildiz, "Channel model and analysis for wireless underground sensor networks in soil medium," Phys. Commun., vol. 3, no. 4, pp. 245–254, Dec. 2010.
[15] X. Dong, M. C. Vuran, and S. Irmak, "Autonomous precision agriculture through integration of wireless underground sensor networks with center pivot irrigation systems," Ad Hoc Netw., vol. 11, no. 7, pp. 1975–1987, 2013.
[16] S. Nie, M. M. Lunar, G. Bai, Y. Ge, S. Pitla, C. E. Koksal, and M. C. Vuran, "mmWave on a farm: Channel modeling for wireless agricultural networks at broadband millimeter-wave frequency," in Proc. IEEE 19th Annu. Int. Conf. Sensing, Commun. Netw. (SECON), 2022, pp. 388–396.
[17] S. M. Hashir, M. C. Vuran, and J. Camp, "ECHO: Empirical characterization and height optimization of UAV-to-underground channels," in Proc. IEEE 34th Annu. Int. Symp. Personal, Indoor Mobile Radio Commun. (PIMRC), 2023, pp. 1–7.
[18] USDA NRCS, "Natural Resources Conservation Service," Accessed: Sep. 13, 2024. [Online]. Available: https://www.nrcs.usda.gov/
[19] H. D. Foth, Fundamentals of Soil Science. United States: 1951.
[20] D. Hillel, Introduction to Environmental Soil Physics. Elsevier, 2003.
[21] K. Roth, R. Schulin, H. Fluhler, and W. Attinger, "Calibration of time domain reflectometry for water content measurement using a composite dielectric approach," Water Resour. Res., vol. 26, pp. 2267–2273, 1990.
[22] I. A. Lunt, S. S. Hubbard, and Y. Rubin, "Soil moisture content estimation using ground-penetrating radar reflection data," J. Hydrol., vol. 307, no. 1–4, pp. 254–269, 2005.
[23] C. Warren, A. Giannopoulos, and I. Giannakis, "gprMax: Open source software to simulate electromagnetic wave propagation for ground penetrating radar," Comput. Phys. Commun., vol. 209, pp. 163–170, 2016.
[24] H. Namdari, M. Moradikia, D. T. Petkie, R. Askari, and S. Zekavat, "Comprehensive GPR signal analysis via descriptive statistics and machine learning," in Proc. IEEE Int. Conf. Wireless Space Extreme Environ. (WiSEE), 2023, pp. 127–132.
[25] J. W. Zhang, S. B. Ye, H. Liu, L. Yi, and G. Y. Fang, "Filtering out antenna effects from GPR data by an RBF neural network," IEEE Geosci. Remote Sens. Lett., vol. 16, no. 9, pp. 1378–1382, 2019.
[26] H.-H. Sun, W. Cheng, and Z. Fan, "Learning to remove clutter in real-world GPR images using hybrid data," IEEE Trans. Geosci. Remote Sens., vol. 60, pp. 1–14, 2022.
[27] USDA NRCS, "Soil bulk density/moisture/aeration," Nutr. Food Sci., vol. 42, no. 4, pp. 11–14, 2012.
[28] Geo LibreTexts, "Soil bulk density," Accessed: Sep. 13, 2024. [Online]. Available: https://geo.libretexts.org
[29] N. R. Peplinski, F. T. Ulaby, and M. C. Dobson, "Dielectric properties of soils in the 0.3-1.3-GHz range," IEEE Trans. Geosci. Remote Sens., vol. 33, no. 3, pp. 803–807, 1995.
[30] Y. Wang, "Frequencies of the Ricker wavelet," Geophysics, vol. 80, no. 2, pp. A31–A37, 2015.
[31] C. A. Balanis, Antenna Theory: Analysis and Design. Hoboken, NJ: John Wiley & Sons, 2016.
[32] A. Géron, Hands-on Machine Learning with Scikit-Learn, Keras, and TensorFlow, 2nd ed., Sebastopol, CA: O'Reilly Media, Inc., 2022.